Supporting Information for

Electrical Programming of Soft Matter: Using Temporally Varying Electrical Inputs to Spatially Control Self Assembly

Kun Yan[§,†,‡], Yi Liu[◊,#,‡], Jitao Zhang[#], Santiago O. Correa[□], Wu Shang[#], Cheng-Chieh Tsai[⊥], William E. Bentley[◊,#], Jana Shen[⊥], Giuliano Scarcelli[#], Christopher B. Raub[□], Xiao-Wen Shi[§,*] and Gregory F. Payne[◊,#,*]

Molecular Modeling

Simulation protocol

A fully extended chitosan chain composed of 20 positively charged glucosamine was built using the CHARMM program (version 38b1[1]) and solvated in a truncated octahedron water box with a minimum distance of 10 Å between the heavy atoms and edges of the water box. The octahedron edge length (lattice parameter) was about 75 Å. Chitosan chain was represented by the modified CHARMM36 carbohydrate force field, as in our previous work.[2] Solvent was represented by the CHARMM-style TIP3P water model.[1] The simulation box was neutralized by adding 20 chloride ions. In the system with 0.5 M salt, 465 sodium and chloride ions were added by replacing solvent molecules at random positions. The total number of water was about 52,000.

All-atom molecular dynamics simulations were performed using GROMACS package version 5.0.[3] The system was first equilibrated for 100 ps under constant temperature and volume (NVT) conditions and heavy atom restrain with a force constant of 1000 kJ mol^{-1} nm^{-2}. The temperature was maintained at 300 K with Nosé-Hoover thermostat using a time constant of 0.1 ps.[4] The equilibration continued for 100 ps under constant pressure and temperature (NPT) conditions at 300 K and 1 bar maintained using the isotropic Parrinello-Rahman pressure coupling method[4] with a time constant of 2 ps and a compressibility of 4.5 $x10^{-5}$ bar^{-1}. Finally, the restraints were released and simulation continued for 100 ns. In all simulations, van der Waals interactions were smoothly switched off from 10 to 12 Å. The particle mesh Ewald method[5] was used to calculate long-range electrostatic interactions with a sixth-order interpolation and 1 Å grid spacing. Bonds involving hydrogen atoms were constrained using the LINCS algorithm[6] to enable a 2-fs time step.

Three sets of simulations were carried out: without salt; with electric field and 0.5 M salt; with electric field and without salt. For each set of simulations, three independent runs with different initial velocity seeds were performed. At the start of each run, the principle axis of the chitosan chain (i.e., chain vector) was aligned with the x-axis. In the simulations with electric field, a uniform electric field of 0.004 V/nm was used. The magnitude of the field is 1000-fold greater than that in the experiment (4×10^{-6} V/nm) to account for the 100-fold smaller molecular mass of the chitosan chain and 10^7-fold shorter simulation time as compared to the experiment. In the three independent runs, the field was applied in the x, y or z direction.

Analysis protocol

The mean squared displacement (MSD) and end-to-end distance calculations were carried

out using g_msd and g_dist modules in GROMACS package version 5.0.4.[3] For simulations with electric field, the MSD in the direction of electric field was calculated as the mass-weighted averages of the MSD's of all atoms in the chitosan chain. For simulations without electric field, the MSD's in x, y and z directions were averaged. The end-to-end distance calculation used the distance between O1 atom on the first glucosamine unit and O4 atom on the last glucosamine unit. For calculations of MSD in the absence of electric field, the MSD in x, y and z directions were averaged. Unless otherwise noted, data from the three independent 100 ns runs were averaged. Post processing of data was carried out using Python scripts. The trajectory snapshots were rendered by Pymol (The PyMOL Molecular Graphics System, Version 1.7 Schrödinger, LLC).

Moving Front Model for Chitosan Segment Growth

Previously, a moving front model has been used to quantify chitosan's segment growth during the on-signal.[7] As illustrated in **Scheme S1**, this moving front model is based on several simplifying assumptions; (i) chitosan is modeled as having two states, fully deprotonated ($Chit^0$) and fully protonated ($Chit\text{-}H^+$); (ii) chitosan's neutralization is responsible for gelation and gelation is rapid such that the growing pH-front and growing gelation-front are co-localized (the region adjacent to the cathode has a $Chit^0$ gel state while the solution contains a $Chit\text{-}H^+$ sol state); (iii) the charge transfer associated with proton consumption at the electrode is equated to the chitosan's deprotonation (i.e., no other buffering species are present); and (iv) chitosan chains undergo no net migration in response to the electrical component of the ON-signal such that the total concentration of chitosan ($Chit^{total} = Chit^0 + Chit\text{-}H^+$) is the same everywhere within the channel (note: this latter assumption is shown to be invalid for solutions lacking salt as the chitosan chains are shown to migrate in response to the imposed electrical potential).

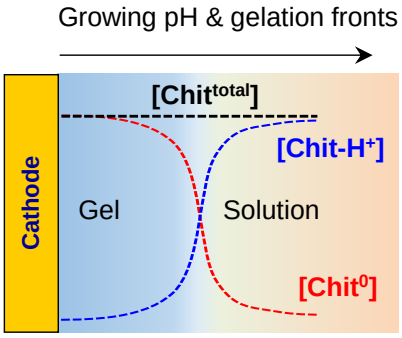

Deprotonation (pH) front:

$$N_{Deprot} = \frac{Q}{F} = \int r_{H^+} dt$$

Gelation front:

$$N_{Gel} = \frac{C \times V_{Gel}}{M} = \frac{C}{M} \times A \times h$$

Co-localization of fronts:

$$N_{Gel} = N_{Deprot} = \frac{Q}{F}$$

Scheme S1. Moving front model for chitosan electrodeposition during the ON-signal. Parameters: charge transfer (Q); Faraday constant (F); current (i); chitosan concentration (C); volume of hydrogel (V); and molecular weight of glucosamine residue (M=161 g/mol).

Chitosan's Deposition in the Absence or Presence of Salt

Experimentally, the channel was filled with a chitosan solution (1%; pH 5.5) containing 20 mM H_2O_2 (cathodic reduction of H_2O_2 allows H^+ consumption without gas bubble generation) and deposition was performed without fluid flow and with a constant ON-signal. **Figure S1** shows that chitosan's deposition in the absence or presence of salt is linear with time and increases with current density consistent with expectations of the moving front model. However, hydrogels grew more rapidly in presence of salt and these differences are illustrated in Figure 2b.

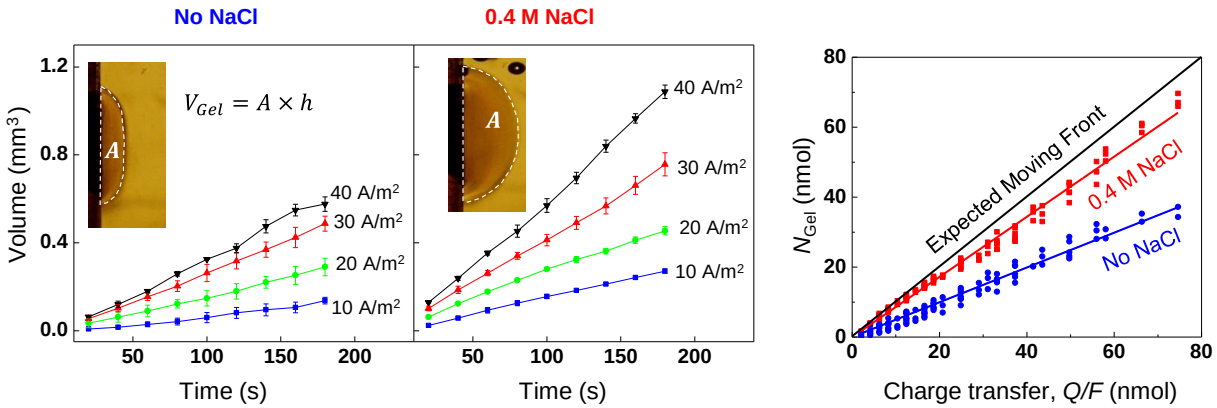

Figure S1. Measured volumes of the growing hydrogel as a function of deposition time and current density.

Evidence that Chitosan Chains Migrate During the ON-Signal

To investigate if chitosan chain migration occurs during the ON-signal, we performed deposition experiments using rhodamine B-labeled chitosan (1%, pH 5.5, 20 A/m^2).[8] **Figure S2** shows that fluorescence images that spanned the channel between the cathode and anode were collected at various times during the ON-signal and the fluorescence intensity distributions across the channel were analyzed. Significant chain migration is apparent when deposition was performed in the absence of salt, while much less chain migration is observed in the presence of salt (this is most obvious from the sequence of images in the anode region).

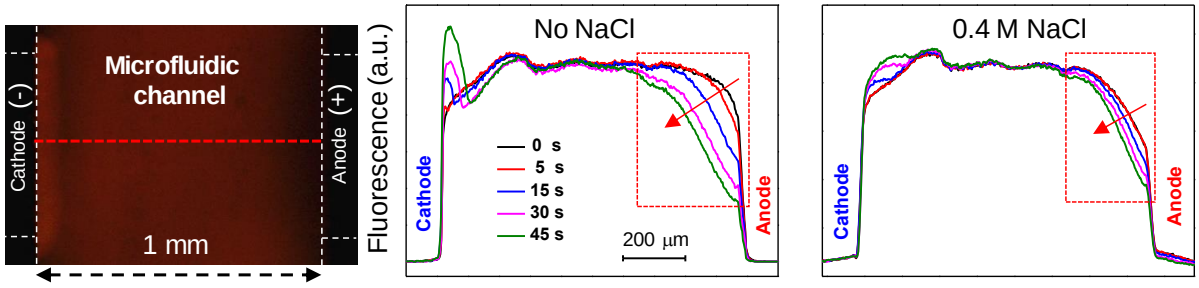

Figure S2. The electrical component of the ON-signal influences the chitosan chains. Fluorescence measurements of rhodamine B labeled chitosan during deposition indicate the chitosan chains can migrate in response to the electric potential during the ON-signal and migration is attenuated in the presence of salt.

Quantitative Polarized Light Microscopy (qPLM)

We used quantitative polarized light microscopy (qPLM)[9-11] to assess the microstructure (i.e., birefringence) of electrodeposited chitosan segment. Specifically, the microfluidic channel with sidewall electrodes was mounted on a rotatable stage of a microscope equipped with crossed polarizers, λ or λ/4-phase shift plates, and a digital camera. The channel was filled with a 1% chitosan solution (pH 5.5) containing 20 mM H_2O_2 and deposition was performed without fluid flow. **Figure S3** shows that before applying an electrical input signal, no birefringence is observed in the chitosan solution, indicating that this solution is isotropic. Two opposing sidewall electrodes (1 mm apart) were then connected to be cathode and anode (CHI6002E

electrochemical analyzer) and electrodeposition was initiated by imposing a constant current density (20 A/m^2). During growth of the chitosan hydrogel film (i.e., segment), time-lapsed birefringence images were collected periodically. The images in Figure S3 show that when electrodeposition was performed in the absence of salt, there is a progressive increase in brightness of the growing chitosan gel, indicating that the chitosan gel has birefringence (i.e., is optically anisotropic). The yellow and blue interference colors were produced when the chitosan chain alignment was parallel and perpendicular, respectively, to the full wave-plate fast axis. Both chitosan alignment and waveplate axes were at 45 degrees with respect to the crossed polarizers. This birefringence is further indicated by the change in interference color observed when the sample was rotated 90° with lambda phase shift plate inserted. In contrast, deposition in the presence of salt shows no evidence of birefringence.

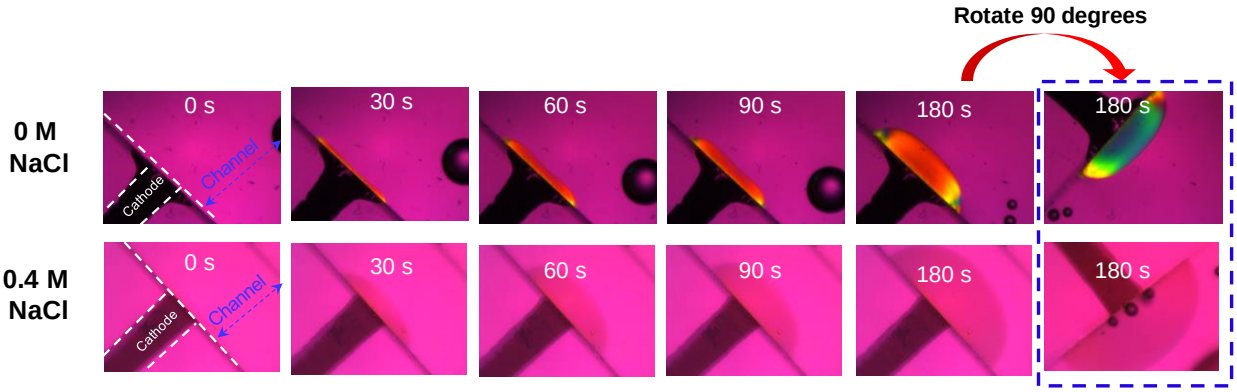

Figure S3. Time-lapsed birefringence images of chitosan gel electrodeposited with a single ON-signal (20 A/m^2) using chitosan solutions (1%, pH 5.5, 20 mM H_2O_2) with no salt or 0.4 M salt. Images were collected with a λ–phase shift plate. [Note: for orientation independent birefringence (OIB) measurements (Figure 2c) a λ/4–phase shift plate was used.] Polarizer and analyzer axes were horizontal and vertical in the image plane, and the lambda-phase shift plate fast axis was oriented diagonally at 45 degrees, from top left to bottom right of the images.

Dissipation of pH Gradient upon Switching the Electrical Signal Off

When the electrical signal is switched from ON to OFF (*i*=0), the steep pH gradient established at the gel-solution interface is expected to gradually relax. To illustrate dissipation of this pH gradient during the OFF-signal we electrodeposited a hydrogel from a chitosan solution (1%, pH 5.5, 20 A/m^2 for 60 s) that contained FITC-dextran (0.15% w/v). These FITC-dextran offer pH-sensitive fluorescence between pH values of 5 and 8.[12, 13] After switching the electrical signal off, fluorescence images were captured sequentially over the course of 2 min. The images were analyzed with ImageJ and the profiles of fluorescence intensity are plotted in Figure 3a. Initially, the strong fluorescence near the cathode indicates the deposited hydrogel exists in a high pH environment (pH > 8). Over time, **Figure S4a** shows a gradual relaxation in the steep pH-gradient at the gel-solution interface. **Figure S4b** is the calibration curve that is used to calculate the dissipated pH over OFF time. **Figure S4c** shows that the hydrogel re-dissolves over prolonged OFF time (e.g., 300 s).

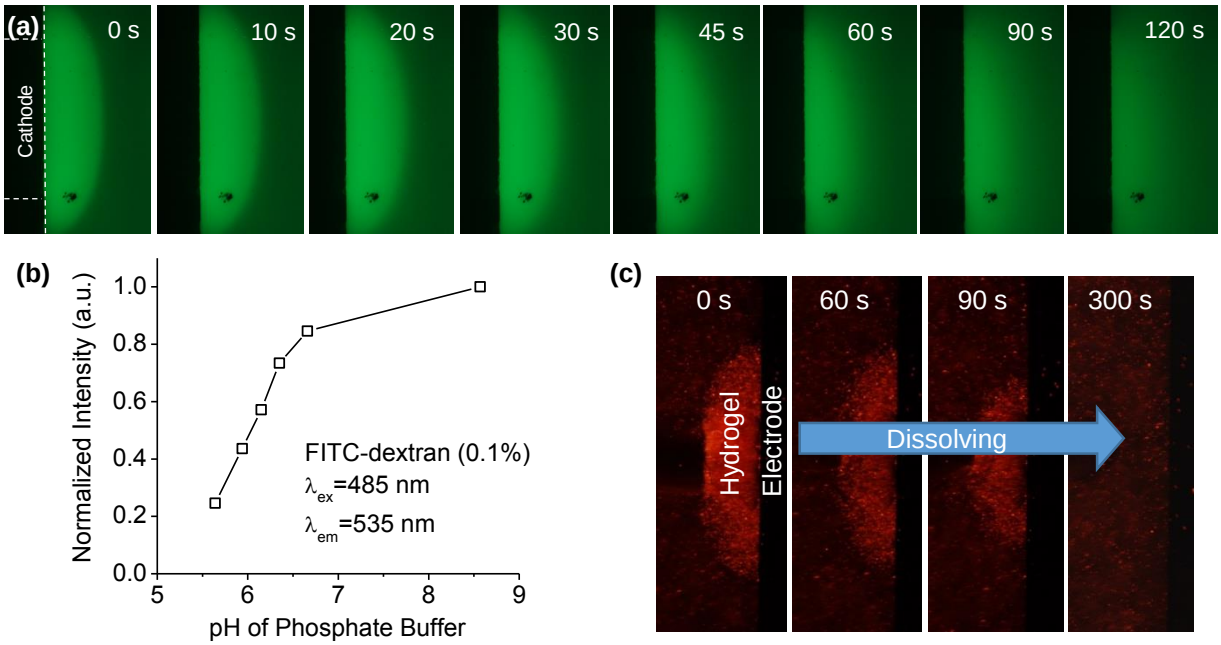

Figure S4. (a) Fluorescence images of pH-sensitive FITC-dextran co-deposited with chitosan immediately after switching the electrical signal from on to off. The steep pH gradient established during the ON-signal is observed to partially dissipate over the course of 2 min. (b) Calibration curve of fluorescence intensity of FITC dextran vs pH of the buffer solution. (c) Fluorescence images of Rhodamine b-dextran (pH-insensitive[14]) co-deposited with chitosan after switching the electrical signal from on to off.

Effect of Resting Potential of the OFF-signal

We tested whether the resting potential of the OFF-signal exerts a sufficient electrical force to influence chitosan chains. Specifically, we filled the fluidic channel with a solution of rhodamine B labeled chitosan and imposed a small constant voltage of -0.5 V (observed current density ≈ 0.009 A/m^2) which was insufficient to induce chitosan's gelation. The fluorescence intensity profiles across the channel are shown in **Figure S5**. These plots indicate some chain migration toward cathode is observed in the absence of salt while little chain migration is observed in the presence of salt.

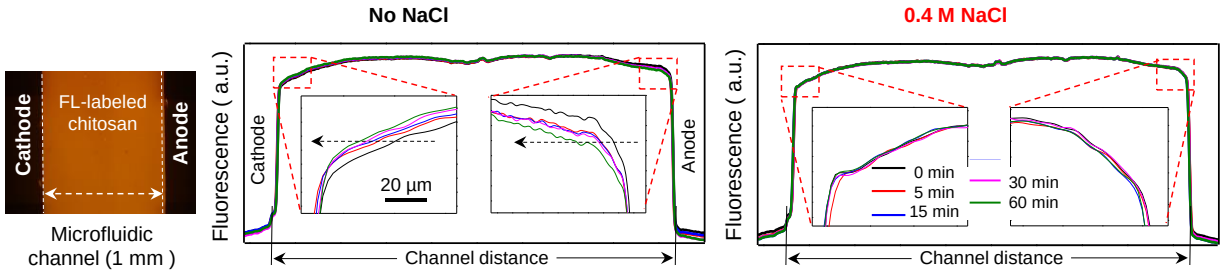

Figure S5. Potentials similar to residual resting potential (-0.5 V) are sufficient to induce chitosan chain migration.

Brillouin Spectroscopy

We first demonstrate that Brillouin scattering spectroscopy has enough sensitivity to detect gelation of the chitosan. As illustrated in Figure 5a, the fluidic channel device was filled with chitosan solution (1%, pH 5.5, 20 mM H_2O_2) and placed on the sample stage of the Brillouin microscope (**Scheme S2**). The laser beam was focused into the center of the channel from bottom, and the focused beam spot was 20 µm away from the cathode in horizontal direction. As soon as an electrical ON-signal was imposed between the cathode and anode (20 A/m^2), the Brillouin frequency shift of the collected backward scattered light was measured continuously at a rate of 20 Hz. To monitor the location where the Brillouin beam probed the sample in real-time, we used a co-registered brightfield microscope. Results from this experiment are shown in Figure 5a and indicate that Brillouin measurements can detect gelation when gels are deposited in the absence of salt but the weak gels formed during deposition of salt[15] cannot be detected by Brillouin measurements.

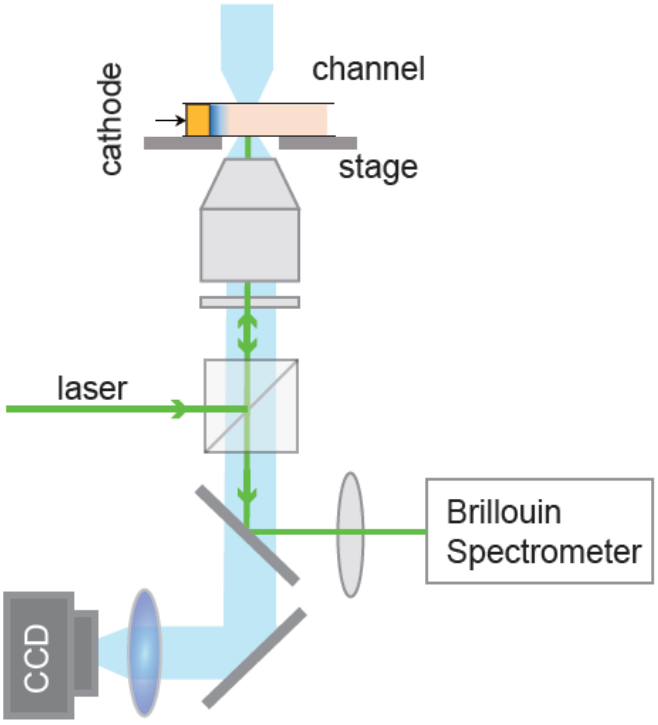

Scheme S2. Schematic illustration of Brillouin microscope. The blue and green beams indicate the optical path of bright-field microscope and of the Brillouin microscope, respectively.

In the subsequent experiment, we imposed oscillating electrical inputs and used Brillouin Spectroscopy to observe segment growth and boundary formation during the ON- and OFF-signals, respectively. Specifically, the fluidic channel device was filled with chitosan deposition solution (1%, pH 5.5, 20 mM H_2O_2), and the device was placed on a microscope-stage and Figure 5b illustrates that the fluidic channel device was scanned repeatedly along the direction of the growing gel to allow the dynamics of hydrogel growth to be monitored in situ. In this experiment, various programmed electrical inputs (ON-signals of 20 A/m^2 for 30 s, and OFF-signals of 0 A/m^2 for 0, 2, 5, 10 s) were applied between the cathode and anode. A total of 5

OFF-steps were included for each input and **Figure S6** shows the time sequence of Brillouin measurements for this experiment. The final scans are shown in Figure 5b.

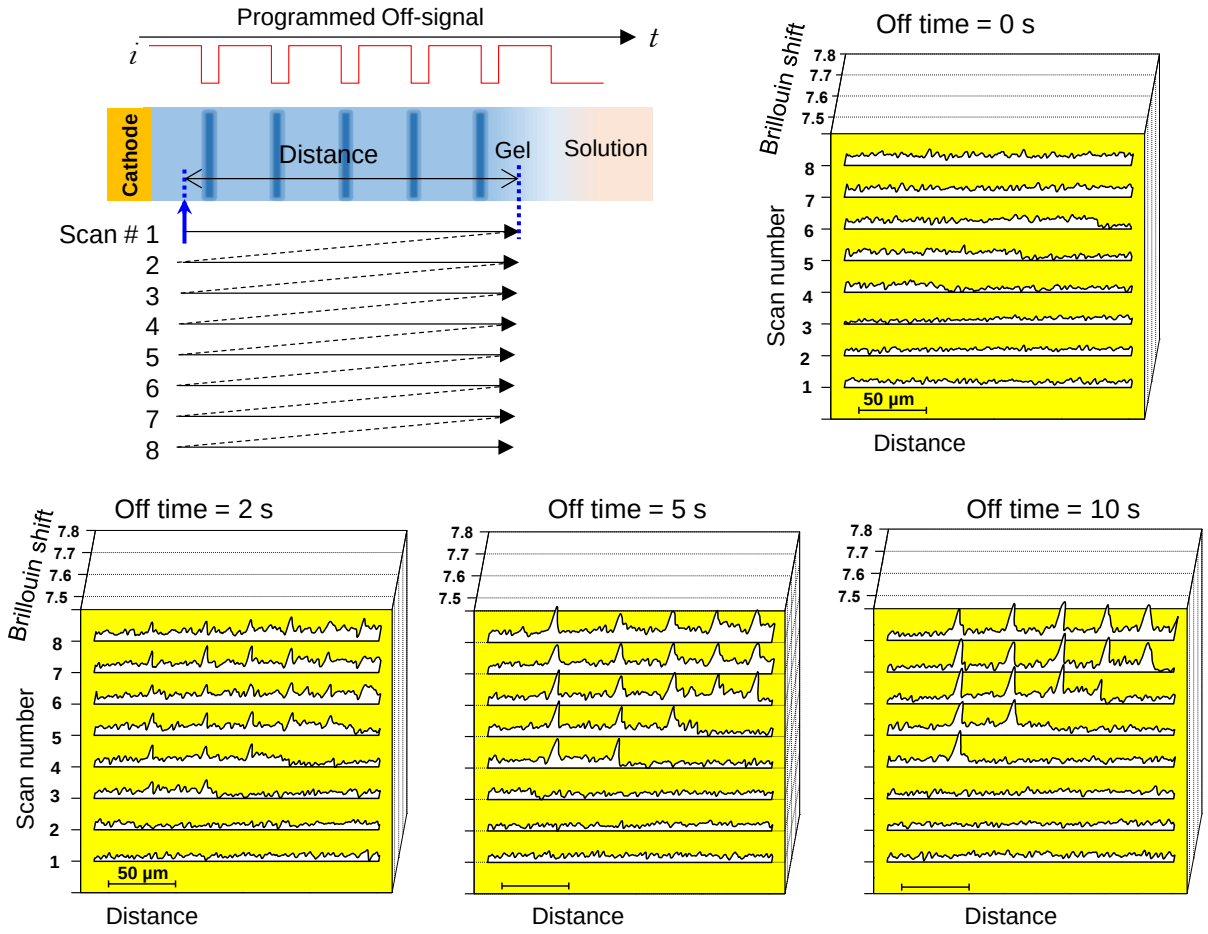

Figure S6. Time-lapsed Brillouin measurements ("waterfall maps") during electrodeposition of chitosan hydrogels generated from chitosan solutions lacking salt using a sequence of ON-signals (20 A/m^2 for 30 s) and OFF-signals of (0 A/m^2 for 0, 2, 5, or 10 s).

For the case that salt was absent from the deposition solution, the Brillouin measurements show distinct spikes emerge from a relatively flat base, and the location of each spike corresponds to one boundary formed during the period of each OFF-signal. The dramatic increases of the Brillouin shift at the boundary regions suggest the moduli of the boundaries are higher than those of segment regions. Moreover, Figure 5b shows that boundaries formed with longer OFF-signals have significantly higher Brillouin shifts (compared to boundaries formed with shorter OFF-signals). On the other hand, when salt was present in the deposition solution, **Figure S7** shows that we did not observe obvious changes of the Brillouin shifts along the gelation direction.

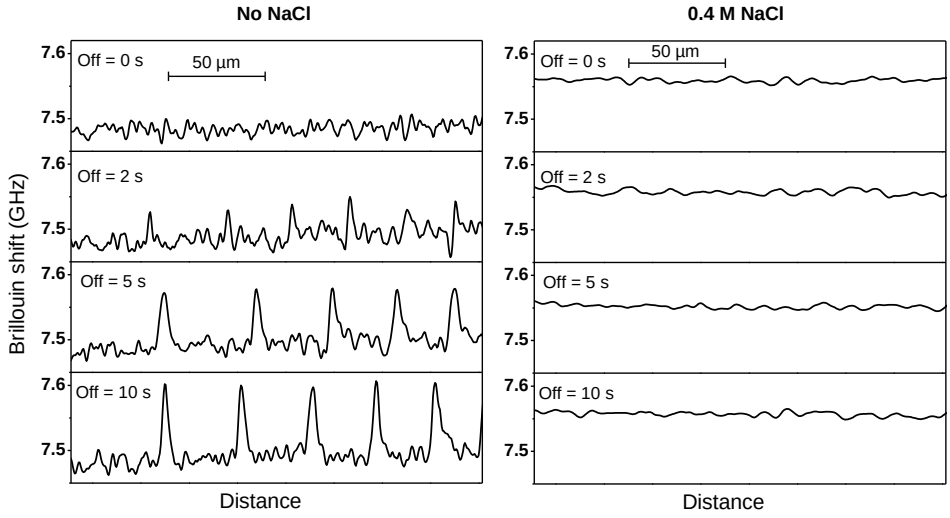

Figure S7. Brillouin measurements of segment growth and boundaries formed with no NaCl (left) and 0.4 M NaCl (right) during various programmed electrical inputs. Hydrogel was deposited from chitosan solutions (1%, pH 5.5, 20 mM H_2O_2, 0.0 or 0.4 M NaCl) using a sequence of ON-signals (20 A/m^2 for 30 s) and OFF-signals of (0 A/m^2 for 0, 2, 5, or 10 s).

Brillouin Measurements of Hydrogels Created with Complex Temporal Electrical Inputs

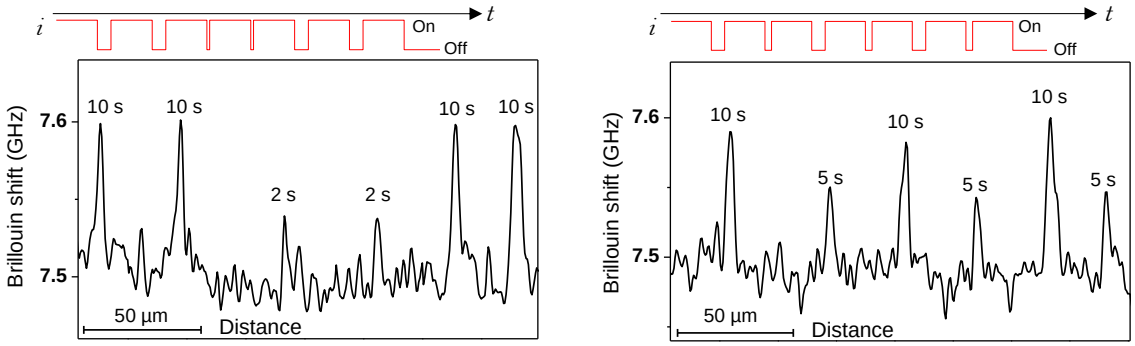

Figure S8. The input curves show that oscillating electrical inputs were programmed to have ON-signals (20 A/m^2) of 30 s duration, and OFF-signals (0 A/m^2) of varying durations. The Brillouin signatures for these patterned structures show that boundary peaks are programmed by the OFF-signal duration with little crosstalk between the ON and OFF signals.

References:

(1) Brooks, B. R.; Brooks, C. L.; Mackerell, A. D.; Nilsson, L.; Petrella, R. J.; Roux, B.; Won, Y.; Archontis, G.; Bartels, C.; Boresch, S.; Caflisch, A.; Caves, L.; Cui, Q.; Dinner, A. R.; Feig, M.; Fischer, S.; Gao, J.; Hodoscek, M.; Im, W.; Kuczera, K.; Lazaridis, T.; Ma, J.; Ovchinnikov, V.; Paci, E.; Pastor, R. W.; Post, C. B.; Pu, J. Z.; Schaefer, M.; Tidor, B.; Venable, R. M.; Woodcock, H. L.; Wu, X.; Yang, W.; York, D. M.; Karplus, M., CHARMM: The Biomolecular Simulation Program. *J. Comput. Chem.* **2009,** *30*, 1545-1614.

(2) Morrow, B. H.; Payne, G. F.; Shen, J., pH-Responsive Self-Assembly of Polysaccharide through a Rugged Energy Landscape. *J. Am. Chem. Soc.* **2015,** *137*, 13024-13030.
(3) Abraham, M. J.; Murtola, T.; Schulz, R.; Páll, S.; Smith, J. C.; Hess, B.; Lindahl, E., GROMACS: High Performance Molecular Simulations through Multi-level Parallelism from Laptops to Supercomputers. *SoftwareX* **2015,** *1–2*, 19-25.
(4) Parrinello, M.; Rahman, A., Polymorphic Transitions in Single Crystals: A New Molecular Dynamics Method. *J. Appl. Phys.* **1981,** *52*, 7182-7190.
(5) Darden, T.; York, D.; Pedersen, L., Particle Mesh Ewald: An N·log(N) Method for Ewald Sums in Large Systems. *J. Chem. Phys.* **1993,** *98*, 10089-10092.
(6) Hess, B.; Bekker, H.; Berendsen, H. J. C.; Fraaije, J., LINCS: A Linear Constraint Solver for Molecular Simulations. *J. Comput. Chem.* **1997,** *18*, 1463-1472.
(7) Yan, K.; Ding, F. Y.; Bentley, W. E.; Deng, H. B.; Du, Y. M.; Payne, G. F.; Shi, X. W., Coding for Hydrogel Organization through Signal Guided Self-assembly. *Soft Matter* **2014,** *10*, 465-469.
(8) Cheng, Y.; Luo, X. L.; Betz, J.; Buckhout-White, S.; Bekdash, O.; Payne, G. F.; Bentley, W. E.; Rubloff, G. W., In Situ Quantitative Visualization and Characterization of Chitosan Electrodeposition with Paired Sidewall Electrodes. *Soft Matter* **2010,** *6*, 3177-3183.
(9) Maki, Y.; Furusawa, K.; Yasuraoka, S.; Okamura, H.; Hosoya, N.; Sunaga, M.; Dobashi, T.; Sugimoto, Y.; Wakabayashi, K., Universality and Specificity in Molecular Orientation in Anisotropic Gels Prepared by Diffusion Method. *Carbohydr. Polym.* **2014,** *108*, 118-126.
(10) Raub, C. B.; Hsu, S. C.; Chan, E. F.; Shirazi, R.; Chen, A. C.; Chnari, E.; Semler, E. J.; Sah, R. L., Microstructural Remodeling of Articular Cartilage Following Defect Repair by Osteochondral Autograft Transfer. *Osteoarthritis Cartilage* **2013,** *21*, 860-868.
(11) Kocsis, K.; Hyttinen, M.; Helminen, H. J.; Aydelotte, M. B.; Modis, L., Combination of Digital Image Analysis and Polarization Microscopy: Theoretical Considerations and Experimental Data. *Microsc. Res. Tech.* **1998,** *43*, 511-517.
(12) Chauhan, V. M.; Burnett, G. R.; Aylott, J. W., Dual-Fluorophore Ratiometric pH Nanosensor with Tuneable pK(a) and Extended Dynamic Range. *Analyst* **2011,** *136*, 1799-1801.
(13) Liu, Y. H.; Dam, T. H.; Pantano, P., A pH-sensitive Nanotip Array Imaging Sensor. *Anal. Chim. Acta* **2000,** *419*, 215-225.
(14) Zheng, X. Y.; Wachi, M.; Harata, A.; Hatano, Y. Acidity Effects on the Fluorescence Properties and Adsorptive Behavior of Rhodamine 6G Molecules at the Air-water Interface Studied with Confocal Fluorescence Microscopy. *Spectroc. Acta Pt. A-Molec. Biomolec. Spectr.* **2004**, *60*, 1085-1090.
(15) Liu, Y.; Zhang, B.; Gray, K. M.; Cheng, Y.; Kim, E.; Rubloff, G. W.; Bentley, W. E.; Wang, Q.; Payne, G. F., Electrodeposition of A Weak Polyelectrolyte Hydrogel: Remarkable Effects of Salt on Kinetics, Structure and Properties. *Soft Matter* **2013,** *9*, 2703-2710.